Metformin-induced longevity is associated with retrotransposon dynamics in yeast chronological aging

Jimena Meneses-Plascencia[1], Ericka Moreno-Méndez[2,3], Diana Ascencio[3], Cesia Pérez-Aguilar[1,3], Michelle Munguía-Figueroa[1], Cei Abreu-Goodger[4], Soledad Funes[2], Alexander DeLuna[1,3,*]

[1] *Unidad de Genómica Avanzada, Cinvestav, 36824 Irapuato, Mexico*

[2] *Departamento de Genética Molecular, Instituto de Fisiología Celular, Universidad Nacional Autónoma de México, 05410 Cd.Mx., Mexico*

[3] *Centro de Investigación sobre el Envejecimiento, Cinvestav, 14330 Cd.Mx., Mexico*

[4] *Institute of Ecology and Evolution, The University of Edinburgh, EH9 3FL Edinburgh, UK*

*Correspondence to: alexander.deluna@cinvestav.mx

Running title: Longevity by metformin and retrotransposons in yeast

Keywords: Metformin; Aging; Retrotransposons; Chromatin regulation; Mitochondria; *Saccharomyces cerevisiae*; Ty1 elements; Chronological lifespan; Set3C histone deacetylase

Highlights

- Large-scale genetic screening reveals that deletions of Set3C histone deacetylase phenocopy metformin-induced longevity.
- Metformin consistently induces Ty1 retrotransposon transcription but reduces Gag protein abundance and retromobility.
- Proteomic changes highlight mitochondrial and stress-response proteins as primary outcomes of metformin exposure.
- Retrotransposon dynamics emerge as a key component associated with metformin-induced longevity.

Abstract

The widely used antidiabetic drug metformin extends lifespan across diverse model organisms, from yeast to primates. However, the cellular mechanisms underlying its anti-aging effects remain only partially understood. Here, we combined large-scale genetic screening and high-resolution lifespan phenotyping with transcriptomic and proteomic analyses to provide a systems view of metformin's impact on the chronological lifespan of *Saccharomyces cerevisiae*. Unexpectedly, we uncovered pronounced gene-drug interactions between metformin and chromatin-modifying factors. Specifically, deletions of Set3C histone deacetylation complex subunits phenocopied the longevity effect of metformin, with no additive benefit when combined, suggesting convergence on shared pathways. Transcriptome profiling further revealed that metformin reprogrammed stationary-phase gene expression, with Ty1-copia retrotransposons emerging as a consistently induced signature, thereby suggesting a possible mechanism for the observed interactions with Set3C regulation. Paradoxically, TYA Gag-like protein levels and retrotransposition frequency were modestly reduced, indicating an uncoupling between transcriptional activation and retromobility. Proteome analysis revealed increased abundance of mitochondrial and stress-response proteins as primary outcomes of metformin exposure, both known modulators of Ty1 dynamics in yeast. Together, our findings position chromatin regulation and retrotransposon expression as integral components of metformin's pro-longevity mechanisms, expanding its influence beyond signaling, metabolism, and stress response.

1. Introduction

Metformin consistently extends lifespan in yeasts, nematodes, and mice (Anisimov et al., 2008; Borklu-Yucel et al., 2015; Onken and Driscoll, 2010; Seylan and Tarhan, 2023; Stynen et al., 2018). It also delays aging phenotypes and improves cognitive function in non-human primates (Yang et al., 2024). The geroprotective potential of metformin is further supported by evidence showing that it attenuates several hallmarks of aging, including impaired nutrient signaling, mitochondrial dysfunction, telomere attrition, cellular senescence, while also promoting autophagy (Barzilai et al., 2016; Kulkarni et al., 2020). Retrospective clinical studies have reported reduced mortality in diabetic patients treated with metformin (Bannister et al., 2014; Campbell et al., 2017). However, more recent analyses suggest that these associations may be affected by biases or confounding factors, contributing to an ongoing debate over the extent of metformin's effects on human longevity (Stevenson-Hoare et al., 2023).

Despite its broad clinical use and pro-longevity potential, our understanding of the molecular mechanisms by which metformin modulates aging remains incomplete. Metformin is widely regarded as an activator of AMPK signaling, which has been linked to lifespan extension (Stancu, 2015; Zhou et al., 2001). It is also well established that metformin accumulates in mitochondria, where it acts as a mild inhibitor of complex I, altering the AMP/ATP ratio and triggering downstream effects including AMPK activation and TOR inhibition (Foretz et al., 2023; Pernicova and Korbonits, 2014; Rena et al., 2017). However, other mechanisms independent of AMPK have been described, including a lysosome-mediated pathway for AMPK and TOR regulation in *Caenorhabditis elegans* (Ma et al., 2022; Zhang et al., 2017), along with downstream outcomes such as improved nutrient sensing, mitochondrial biogenesis, SIRT1 activation, and increased autophagy (Kulkarni et al., 2020). In parallel, AMPK-independent effects of metformin also include reduced reactive oxygen species (ROS), anti-inflammatory signaling via NF-κB and Nrf2-Gpx7, and the activation of DNA damage response pathways such as ATM kinase (Kulkarni et al., 2020).

The budding yeast *Saccharomyces cerevisiae* has emerged as a key model for studying the biology of aging (Kaeberlein, 2010), helping identify molecular factors that modulate aging and longevity in both this unicellular organism and more complex eukaryotes (Fabrizio and Longo, 2003; Janssens and Veenhoff, 2016). It also represents a powerful platform to characterize the mechanisms associated with potential anti-aging compounds (Zimmermann et al., 2018). However, few studies have systematically explored how metformin extends lifespan in yeast aging models. Transcriptome analyses in *S. cerevisiae* show that both glucose limitation and metformin enhance chronological lifespan (CLS), likely via improved mitochondrial function and mitochondria-to-nucleus signaling (Börklü, 2023; Borklu-Yucel et al., 2015). CLS extension by metformin in yeast is also linked to reduced advanced glycation end products and downregulation of mitochondrial respiration proteins (Kazi et al., 2017). Moreover, large-scale homomer dynamics screens suggest that metformin triggers a cellular response resembling iron deficiency (Stynen et al., 2018). In the fission *Schizosaccharomyces pombe*, metformin increases glucose consumption and ATP production while lowering ROS, indicating enhanced metabolism and oxidative stress resistance (Seylan and Tarhan, 2023). Still, an integrated mechanistic view remains elusive, and key molecular players may yet be unidentified, given the widely recognized pleiotropic nature of metformin's cellular effects.

In this study, we investigated the mechanisms underlying metformin-induced chronological longevity of yeast cells by combining large-scale genetic screening with transcriptomic and proteomic analyses. We found that metformin extends CLS through mechanisms independent of pH buffering, involving stress responses, mitochondrial function, and an unexpected involvement of the SET3C histone deacetylase complex, which had not been previously linked to metformin's effects. Notably, we identified a novel connection between metformin treatment and Ty1 retrotransposon regulation, whereby metformin increased Ty1 expression without promoting its mobility, suggesting that retrotransposon dynamics contribute to its anti-aging effects.

2. Materials and Methods

2.1. Strains and media. Large-scale competitive-aging screening was carried out with a set of 1438 strains deleted for genes with at least one ortholog in human. Orthologs were defined with the BioMart tool from Ensembl (Kinsella et al., 2011). A collection of haploid strains tagged with mCherry red fluorescent protein (RFP) was generated by crossing viable BY4741 deletion strains (*MAT*a *xxx*Δ::*kanMX4 his3*Δ*1 ura3*Δ*0 leu2*Δ*0 met15Δ0*) with the Y8205-RFP SGA-starter strain (*MAT*α *PDC1-RFP-CaUR*A3 *his3*Δ*1 ura3Δ0 can1*Δ*::STE2pr-SpHIS5 lyp1*Δ). The resulting prototrophic haploid progeny had the following genotype: *MAT*a *xxx*Δ*::kanMX4 PDC1-RFP-CaURA3MX4 can1*Δ*::STE2pr-SpHIS5 lyp1*Δ *LEU2 his3*Δ*1 ura3*Δ*0*. WT reference strains had insertions at the neutral *his3*Δ locus, tagged with Cerulean (CFP) or mCherry (RFP). The *RFP*-tagged *his3*Δ reference was also used as the WT for transcriptomic profiling by RNA-seq.

For large-scale flow-cytometry proteomics, a subset of 2600 strains from the GFP fusion collection (Huh et al., 2003) was used; selection included all strains with detectable flow-cytometry GFP signal (Newman et al., 2006). Selected GFP strains were crossed with the strain *Mat*α *ho*Δ::*BFP-G418 HIS3::HYG* resulting in an array of strains with genotype: *Mat*α *XXX-GFP-HIS3Mx6 ho*Δ::BFP-G418 *can1Δ::CaUra3 lyp1Δ::STE3pr_LEU2 his3*Δ::*HYG.*

All chronological lifespan assays were carried out in synthetic complete medium (SC) medium buffered to pH 4 (citrate-phosphate buffer), unless otherwise noted. SC medium contained 2% glucose, 0.2% complete amino acid mix, 0.67% yeast nitrogen base (YNB) without amino acids, 30 mM citric acid, and 18.5 mM sodium citrate. Where indicated, metformin (Sigma D150959) was added to the medium to final concentrations ranging from 3 to 200 mM. Outgrowth medium was low-fluorescence YNB (Sheff and Thorn, 2004).

2.2. High-throughput CLS screening by competitive-aging. Mutant-RFP arrays and WT-CFP were grown separately until saturation and then mixed in a 2:1 ratio. Mixed cultures were

94 replicated by pinning into a 96 semi-deep-well with 750 µL SC medium (pH 4), with or without 50
95 mM of metformin. Cultures were incubated without shaking at 30 °C and were sampled during
96 stationary phase for nine consecutive days, starting at 60 h after inoculation. Ten microliter
97 aliquots were used to inoculate 140 µL of fresh YNB low fluorescence medium employing a 96-
98 channel pipetting arm. Outgrowth kinetics were monitored every 1.5 h for 15 h by recording
99 absorbance at 600 nm (OD600*nm*) along with raw fluorescence of *RFP* (Ex 587/5 nm, Em 610/5
100 nm) and *CFP* (Ex 433/5 nm, Em 475/5 nm) using a Tecan Infinite M1000 reader integrated to a
101 cell-assay robotic platform (Tecan Freedom EVO200). Optimal gain was calculated before the
102 start of each batch experiment.

103 **2.3. Data normalization and analysis.** The survival coefficients (*S*) of each sample relative to
104 the WT reference was estimated by fitting the data to a multiple regression model, as reported
105 (Avelar-Rivas et al., 2020). MATLAB scripts are available at
106 https://abrahamavelar.github.io/LinearModelCLS/. Raw survival coefficients were normalized for
107 batch effects by subtracting the median *S* of each plate. The final CLS normalized dataset is
108 provided in **Table S1**. CLS screening also included a total of 227 reference samples, in which an
109 RFP-tagged WT was aged in competition with a CFP-tagged WT. The distribution of these
110 reference samples was used to compute a Z-score and associated *p*-value for each mutant tested
111 (normally distributed x^2 test, p=0.16 and p=0.29 for –MTF and +MTF, respectively). Short- and
112 long-lived phenotypes in each condition were defined after correcting for multiple hypotheses
113 testing (*FDR, q*<0.05).

114 Lifespan extension by metformin (LE_{MTF}) was defined as:

115 $$LE = \frac{S_{MTF} + 1}{S_{SC} + 1}$$

116 Likewise, diminished or enhanced lifespan extension was determined by assigning each mutant
117 a *Z*-score from the *LE* distribution of the 227 WT reference replicates (normally distributed, p=
118 0.19, x^2 test) and corrected for multiple hypothesis (q<0.05, Benjamini–Hochberg FDR).

119 **2.4. Functional enrichment analysis.** To identify gene sets with atypical *LE* median values, all
120 genes tested were grouped by their annotated GO terms; only those groups with at least 5 genes
121 and no more than 50 genes measured were considered. Annotation files were downloaded from
122 the Yeast Genome Database (2023). The distribution of *LE* values within each group was
123 compared to the distribution of all deletion strains tested. Gene sets associated with longevity by
124 metformin were defined as those with a median *LE* value different to the entire data set (Wilcoxon
125 rank sum test, p<0.05). Significant gene sets and the genes within each set are listed in **Table**
126 **S2**.

127 **2.5. Validation of CLS phenotypes by live/dead staining.** Selected strains were pre-cultured
128 for 36 h in 96-well plates (Corning 3585). Saturated cultures were pinned into 96 semi-deep-well
129 plates containing 750 µL SC medium (pH 4), with or without metformin. Cultures were incubated
130 without shaking at 30 °C. After 48 h, 6 µL samples were taken using a Tecan Freedom EVO200
131 robotic arm and transferred to 96-well plates with 50 µL of staining solution (3.34 µM propidium
132 iodide and 20 µM Syto9; LIVE/DEAD™ FungaLight™ Yeast Viability Kit). Live cells were
133 quantified by flow cytometry (LSRFortessa™, BD), using Syto9-positive events. Propidium iodide
134 was excited at 561 nm (586/15 BP filter), and Syto9 at 488 nm (525/50 BP, 505LP filters). Survival
135 curves were fitted with an exponential decay model to estimate half-life, and survival integrals
136 were calculated as the area under the curve for each independent experiment. Statistical
137 differences of 50 mM treatment compared to the –MTF control were assessed by unpaired two-
138 tailed Student's t-test (p < 0.05).

139 **2.6. Proteomic response to metformin measured by analytical flow cytometry.** GFP-tagged
140 strains were pre-cultured for 36 h in 96-well plates (Corning 3585). Using a Tecan Freedom
141 EVO200, 10 µL of each saturated culture was transferred into 96 semi-deep-well plates containing
142 750 µL SC medium (pH 4), with or without metformin. Cultures were incubated at 30 °C without
143 shaking for 24 h, 48 h, or five days, as indicated. At each time point, 10 µL samples were mixed
144 with 50 µL Tris-EDTA buffer in 96-well plates and analyzed by flow cytometry (LSRFortessa™,
145 BD). GFP was excited with a 488 nm laser, and emission was detected using a 525/50 band-pass
146 filter. Doublets were excluded using side scatter (SSC), and median GFP fluorescence was
147 calculated from singlet events. Log2 fold changes were estimated as the protein-abundance
148 change ratio under each treatment. Functional analysis was performed as described previously
149 for *LE* values, by comparing the distribution of Log2 fold changes of each gene set to that of the
150 complete set of 2616 GFP-fusion strains sampled.

151 **2.7. RNAseq and data analysis.** Pre-inoculums of the WT strain were established by culturing
152 5–6 individual colonies in 10 mL of SC medium (pH 4) at 30 °C with shaking (200 rpm) for 24 h.
153 Cultures were then diluted to an OD_{600} of 0.05 in 50 mL of SC medium (pH 4), with or without
154 metformin, and incubated under the same conditions. Cells were collected at mid-exponential
155 phase (OD_{600} = 0.5) and late stationary phase (8 days), with 10^7 cells/mL harvested per replicate.
156 Total RNA was extracted using the RiboPure™ Yeast Kit (Invitrogen AM1926). Four replicates
157 from the exponential phase and five from the stationary phase were used for directional, rRNA-
158 depleted, 150 bp paired-end sequencing (Novogen).

159 Low-quality bases and adapter sequences were trimmed using FASTP. Trimmed reads were
160 aligned to the reference genome using STAR and filtered by mapping quality with Samtools.
161 Read counts were obtained using HTSeq. Data normalization was performed with the RUVseq
162 package, and differential expression analysis was conducted using DESeq (FDR < 0.1,
163 Benjamini-Hochberg) in RStudio. GO over-representation analysis was carried out using the

164 enrichGO function from the clusterProfiler package. A Jaccard index and hierarchical clustering
165 were applied to the resulting GO terms, and functional networks were constructed in Cytoscape
166 (v3.10.2).

167 **2.8. Retromobility assay.** A Ty1his3-AI retrotransposon reporter strain was obtained by lithium-
168 acetate transformation of the BY4741 strain with a centromeric plasmid construction that
169 contains a Ty1 element with its native promoter (Hénault et al., 2020). The construction carried
170 the YMRCTy1-3 Ty1 element (YMR045C). The TYA Gag and TYB Pol coding regions of this
171 LTR retrotransposon were chosen because of their significant upregulation by 50mM metformin
172 compared to the –MTF control (0.47 log2 fold change; p=0.002, Benjamini-Hochberg FDR).

173 Ty1 his3-AI mobility frequency was assayed as previously described (Nyswaner et al., 2008),
174 with modifications. Starting cultures of the Ty1 reporter strain were initiated by inoculating 10 mL
175 of SC medium (pH 4) with three isolated colonies and incubating at 30 °C with shaking (200 rpm)
176 for 24 h. Saturated cultures were diluted 1:1000 into 25 mL of fresh SC medium (pH 4), with or
177 without metformin, and incubated at 20 °C with shaking (100 rpm) for 75 h to allow
178 retrotransposition. To estimate colony-forming units (CFUs), serial dilutions were prepared and
179 100 µL of the 10^{-5} dilution was plated on YPD agar. In parallel, 12 mL of each culture was
180 centrifuged (2000 × g, 10 min, RT), washed twice, and resuspended in 2 mL of sterile water.
181 Cells were plated on SC–His agar using a sterile glass spreader and incubated at 30 °C for 48 h
182 (CFU) or 72 h (His^+ colony counting). Retrotransposition frequency was calculated by dividing
183 the number of His^+ colonies by CFUs per µL.

184 # 3. Results

185 ## 3.1. Metformin increases chronological longevity under pH-buffered conditions

186 Metformin has been shown to increase the chronological longevity of *S. cerevisiae* (Borklu-Yucel
187 et al., 2015; Stynen et al., 2018). However, metformin also prevents pH acidification of stationary
188 phase cultures in conventional SC medium (Avelar-Rivas et al., 2020). Since acetic acid-induced
189 mortality is a major driver of chronological aging under non-buffered conditions (Burtner et al.,
190 2009; Ludovico et al., 2001), the buffering effects of metformin may explain its impact on
191 chronological survival. We thus set out to evaluate the effects of metformin on the CLS
192 phenotype of cells aged under buffered-media conditions. To determine an optimal pH for CLS
193 profiling, we first evaluated the effects of the drug on the growth kinetics of a WT strain grown
194 under SC media buffered at a range of pH (**Figure S1**). We observed that high doses of
195 metformin had little to no effect on cell growth at a pH range of 3 to 5, while cells grown at higher
196 pH values showed increased sensitivity as a function of drug concentration. Based on this result,
197 we reasoned that stationary-phase survival would be better assayed in media buffered at pH 4
198 in which cells grow at their normal rates.

199 To assess the chronological-aging effects of metformin under buffered conditions, we used
200 live/dead staining coupled to flow cytometry to characterize the CLS of cells aged on SC medium
201 buffered at pH 4 under increasing concentrations of the drug (**Figure 1A**). We observed that
202 metformin led to increased chronological longevity in a dose-dependent manner. Specifically,
203 the half-life of the WT increased from 25 days in the control to up to 41 days in the 75 mM
204 treatment (39% CLS increase) (**Figure 1B**). We also observed that metformin was rendered
205 deleterious at high doses, with a half-life reduction to 17 days in the 200 mM treatment (41%
206 decrease). These results show that metformin can increase chronological longevity in buffered
207 conditions, suggesting that part of the cellular mechanisms of longevity by metformin in yeast
208 are independent of its buffering capacity.

209 **3.2. Large-scale genetic profiling of aging in metformin**

210 To systematically identify genetic factors underlying lifespan extension by metformin in budding
211 yeast, we carried out a large-scale functional genomics aging assay. Specifically, we screened
212 a set of 1438 knockout strains from the yeast deletion collection, which included most non-
213 essential genes having at least one human ortholog (Kinsella et al., 2011). To this end, we used
214 a sensitive competitive-aging assay developed in our laboratory, which tracks changes in
215 stationary-phase viability of gene-deletion strains aged in coculture with a fluorescently tagged
216 WT reference (**Figure 2A**) (Avelar-Rivas et al., 2020; Campos et al., 2018; Garay et al., 2014).
217 With this approach, we obtained a relative survival coefficient for each knockout strain aged with
218 50 mM metformin (+MTF) or without the drug (–MTF) (**Figure 2B**). Survival coefficients were
219 normalized to account for batch effects by subtracting the median raw value of each plate
220 (**Figure S2**). Importantly, a subset of 84 mutant strains was assayed under both conditions in
221 five independent experiments, showing high replicability in the survival coefficients measured (r
222 =0.90–0.97; **Figure S3**). All large-scale genetic screening data is provided in the Supporting
223 Information (**Table S1**).

224 To score gene-deletion strains with increased or decreased CLS under each treatment, the
225 distribution of the survival coefficients of all deletion strains was compared to a null distribution
226 of 227 WT strains. In the control SC medium without the drug, 261 (18.2%) deletion strains
227 showed significantly decreased lifespan, while 36 (2.5%) mutants showed increased lifespan
228 compared to the WT (**Figure 2B**). The number of significant CLS effects in the +MTF treatment
229 were 291 (20.2%) and 17 (1.18%) for short- and long-lived deletion strains, respectively (**Figure**
230 **2B**).

231 To validate results of our CLS genetic screens, we used live/dead staining to estimate the CLS
232 phenotype of a subset of deletion strains assayed at smaller scale. This set included strains that
233 were top hits under at least one of the two conditions, which also allowed testing for false

234 negatives given that many of the CLS phenotypes were only observed under one condition. Our
235 validation experiments showed that, without metformin, 16 out of 26 (62%) strains recapitulated
236 their neutral CLS phenotype, while 18 / 28 (64%) and 5 / 5 (100%) recapitulated their short- and
237 long-lived CLS phenotypes, respectively, when tested by live/dead staining (**Figure 2C**).
238 Likewise, 19 / 27 (70%), 21 / 31 (68%), and 1 / 1 (100%) deletion strains showed consistent
239 neutral, short-, and long-lived CLS phenotypes when retested in the presence of metformin.
240 Selected validation experiments are shown in **Figure 2D**; all hits tested are provided in **Figure**
241 **S4**. The rate of validation of hits in our large-scale screens is similar to that reported in previous
242 CLS surveys (Campos et al., 2018; Matecic et al., 2010). These results indicate that our
243 competitive aging approach yields an accurate estimation of CLS under different conditions,
244 allowing us to further describe gene-drug interactions and their role in lifespan extension by
245 metformin.

246 **3.3. Altered chromatin organization phenocopies the longevity effect of metformin**

247 To gain deeper insight into the genes and cellular processes underlying metformin's lifespan-
248 extending effect, we analyzed our large-scale genetic data to identify deletions that alter
249 survival coefficients under metformin treatment relative to drug-free medium. To this end, we
250 calculated a relative lifespan extension coefficient (LE_{MTF}) for each deletion strains, which
251 provides a metric to identify genes associated with diminished or enhanced relative lifespan
252 extension upon treatment with metformin. Using a 5% FDR cutoff, we found that 45 deletion
253 strains showed decreased LE_{MTF}, whereas 24 lived significantly longer under metformin
254 treatment (**Figure 3A**). Deletion of *TPK1*, which encodes a catalytic subunit of PKA, showed
255 diminished lifespan extension, whereby its short-lifespan phenotype was strongly aggravated by
256 metformin. This supports a requirement for intact PKA signaling in metformin-induced longevity,
257 consistent with its archetypical mechanisms of action. Unexpectedly, other top hits with
258 diminished lifespan extension included strains impaired in chromatin regulation. For example,

259 deletions of *SNT1* or *HST1*, coding for subunits of the Set3C histone deacetylase complex,
260 extended lifespan in drug-free medium but were rendered neutral or detrimental in the presence
261 of metformin. These kind of alleviating gene-drug interactions suggest that the longevity effects
262 of gene deletions and metformin treatment arise from common underlying mechanisms.

263 To better resolve the cellular functions underlying metformin-induced longevity, we used our
264 quantitative dataset to search for GO terms with significant skew in their distributions of LE_{MTF}
265 values. This quantitative analysis avoids reliance on arbitrary cutoffs and can reveal functional
266 groups enriched in genes with milder effects that would be missed by standard significance
267 thresholds. Using this strategy, we identified several processes consistently linked to metformin
268 action across model organisms, including PKA signaling, mitochondrial function, and redox
269 metabolism (**Figure 3B**; **Table S2**). In addition, cellular proteostasis, vacuole function, and the
270 extracellular space were also hits showing significant deviation in their median LE_{MTF} values.
271 Noteworthy, impairment of Set3C chromatin modification proved to be the top hit of gene
272 deletions consistently associated with diminished longevity by metformin.

273 We focused on the unexpected link of the Set3C histone deacetylation complex with the
274 cellular response to metformin, which was the top functional hit enriched in negative gene-
275 drug interactions. In *S. cerevisiae*, this complex includes 7 non-essential subunits; it is the
276 yeast analog of the mammalian HDAC3/SMRT complex (Pijnappel et al., 2001). Using
277 live/dead staining of stationary-phase cells aged in individual cultures, we re-evaluated the
278 genetic interactions of all Set3C subunit deletion strains aged with and without metformin
279 (**Figure 3C**). This validation experiment included single deletions of *SET3* and *HOS2*, which
280 were not part of the original large-scale screen due to the absence of direct human orthologs.
281 With the sole exception of Δ*cpr1*, all Set3 complex subunits mutants showed diminished
282 lifespan extension, whereby the strong long-lived phenotypes of the deletion strains were
283 partially suppressed in cells aged with metformin. Significant negative gene-drug

284 interactions—defined as diminished lifespan extension in response to metformin—were
285 observed for *HOS4*, the histone deacetylases *HST1* and *HOS2*, and *SNT1*, the scaffold
286 component of Set3C. This pattern of diminished lifespan extension suggests that impaired
287 Set3C chromatin regulation and metformin treatment act through overlapping pathways that
288 promote chronological longevity. In this context, Set3C deletions phenocopy the longevity
289 effect of metformin, and no additive effect is observed when both interventions are combined.
290 Our large-scale genetic interaction analyses reveal consistent and reproducible gene-drug
291 interactions between Set3C components and metformin.

292 **3.4. Metformin leads to increased expression of Ty1 retrotransposons in aging cells**

293 To shed light into the nature of the overlapping regulatory pathways linking the cellular
294 responses to metformin and impaired Set3C chromatin, we carried out a global transcriptomic
295 analysis. Specifically, we performed RNAseq analysis comparing populations of WT cells in mid
296 exponential and late stationary phase with or without metformin. As expected, PCA analysis of
297 replicated samples showed a strong signal clustering stationary-phase cells apart from
298 exponential-phase cells, and a moderate clustering of metformin treated cells, but only in
299 stationary phase (**Figure 4A**). Despite its impact on chronological lifespan, metformin had a
300 relatively modest effect on the stationary-phase transcriptome, with significant expression
301 changes detected in only 3.0% of genes. After performing a differential expression analysis for
302 stationary phase cells, we found that metformin resulted in significant upregulation of 154 genes
303 and downregulation of 25 genes (p<0.05, Benjamini-Hochberg FDR adjusted) **(Figure 4B**;
304 **Table S3**).

305 To provide a functional description of the biological processes involved in transcriptional
306 reprogramming promoted by metformin, we conducted a GO enrichment analysis of the
307 identified set of up and down-regulated genes (**Table S4**). GO groups were clustered based on

308 their gene-content similarity, using the Jaccard index among the ensuing terms (**Figure 4C**).
309 Our analysis showed that metformin resulted in increased expression of several gene sets with
310 roles on stress response, such as osmotic stress, oxidative stress, heat shock and protein
311 folding, carbohydrate metabolism, and trehalose accumulation. Strikingly, our results showed
312 that the transcription of Ty retrotransposon genes increased when cells were aged in the
313 presence of metformin (**Figure 4D**). A closer inspection of the transcriptional changes of
314 different retrotransposon families revealed that this effect was stronger for members of the Ty1-
315 copia group of retrotransposons (**Figure 4E**). Because Set3C components regulate Ty1 activity
316 in yeast (Mou et al., 2006), our findings suggest that both impaired Set3C function and metformin
317 treatment influence Ty1 expression, which may underlie the previously noted phenocopying of
318 metformin-induced longevity by Set3C deletions.

319 **3.5. Metformin result in decreased levels of retromobility and TYA Gag-like protein,**
320 **despite increases in Ty1 transcriptional expression**

321 Based on the observed increases of Ty1 retrotransposons expression upon treatment with
322 metformin, we asked whether metformin also resulted in increased retromobility and integration
323 into the genome. To answer this question, we used a plasmid-borne Ty1his3AI reporter bearing
324 the sequence of the *YMRCTy1-3* element of *S. cerevisiae* (Hénault et al., 2020). After incubating
325 WT cells at a permissive temperature for retrotransposition, we found that the transposition rate
326 showed a modest two-fold decrease in cells treated with higher doses of metformin (**Figure 4F**).
327 While this decreased rate of retromobility was not significant because of the high variability
328 observed in untreated cells, it was surprising given that the same drug dose lead to increased
329 Ty1 transcriptional expression.

330 To confirm the paradoxical pattern of robust Ty1 induction alongside a modest reduction in
331 retromobility, we used the *YDR170-W* Ty1 locus as a TYA-GFP fusion reporter to track changes
332 in the abundance of the TYA Gag-like protein in the transition to stationary phase. The TYA

333 protein is analogous to the Gag protein of retroviruses and is essential for the formation of virus-
334 like particles during the yeast retrotransposon replication cycle (Brookman et al., 1995). In
335 agreement with reduced levels of retromobility, we found that treatment with metformin resulted
336 in reduced levels of the TYA-GFP reporter, which was significant during post diauxic growth and
337 early stationary phase at 12 and 24 hours in culture, respectively (**Figure 4G**). These results
338 suggest that increased expression of Ty1 elements by metformin leads to increased genome
339 stability defined as reduced rates of Gag-like protein and retromobility. Together, these findings
340 reveal a previously unappreciated role for metformin in modulating retrotransposon activity,
341 suggesting that enhanced Ty1 transcription may paradoxically contribute to genome stability by
342 suppressing later steps of the retrotransposition cycle.

343 **3.6. Metformin increases the abundance of proteins involved in mitochondrial function**
344 **and stress-response**

345 To further explore the cellular pathways through which metformin promotes longevity, beyond
346 the genetic associations with Set3C and the transcriptional activation of Ty1 elements, we
347 examined the dynamics of the proteome during the transition into stationary phase. This
348 approach was aimed at identifying broad cellular targets of metformin that could contribute to
349 downstream effects on retrotransposon activity and longevity. To this end, we used the GFP
350 fusion collection coupled with flow cytometry to track changes in protein abundances (DeLuna
351 et al., 2010; Newman et al., 2006). We first measured a subset of GFP fusions harvested at
352 different times culture with or without metformin (**Figure S5**). The correlation between different
353 replicate experiments was high at early stationary phase (24 and 48 h incubation) and
354 decreased later in stationary phase (5 d), likely due to reduced GFP fluorescence signal during
355 starvation (Roberts et al., 2016). Based on these observations, we screened the GFP collection
356 focusing on cells at early stationary phase (24 h). Strains with undetectable fluorescence
357 intensity in nominal conditions (Newman et al., 2006) were filtered out, resulting in a final dataset

358 consisting of 2616 GFP fusion strains (**Table S5**). Finally, we estimated the median intensity
359 fluorescence of each strain for the two conditions after removing doublets, which were the
360 absolute protein expression levels of each gene in cells with and without metformin.

361 Our proteome analysis revealed that most GFP fusions were unaffected by metformin (**Figure**
362 **5A**). However, a subset of strains showed significantly increased or decreased reporter levels,
363 such as the stress-induced cell wall glycoprotein Sed1 and the Gus1 Glutamyl-tRNA synthetase,
364 respectively. We grouped the GFP fusion strains by their annotated GO term and compared the
365 fold-change distribution of each group with the distribution of the 2616 strains tested. We found
366 that metformin led to increased abundance of proteins with roles on removal of superoxide
367 radicals, protein folding, and carbohydrate storage (**Figure 5B**), which agreed with our
368 transcriptome screening. Likewise, proteins related to mitochondrial respiration and amino acid
369 and fatty acid metabolism were also increased. Given that mitochondrial activity and ROS are
370 known to impact Ty1 dynamics (Stoycheva et al., 2007; VanHoute and Maxwell, 2014), these
371 changes may provide a link between metformin-induced mitochondrial remodeling and the
372 observed upregulation of Ty1 elements. Conversely, the levels of proteins associated with DNA
373 replication, RNA processing, filamentous-growth signaling, and aminoacyl-tRNA metabolism
374 were reduced in response to metformin. The absence of clear functional groups related to Set3C
375 or other chromatin-modifying complexes in our proteome dataset further supports the view that
376 Set3C and metformin act indirectly through convergent effects, possibly mediated by changes
377 in Ty1 expression. Overall, our proteomic survey indicates that metformin directly impacts
378 mitochondrial activity, metabolism, and stress-response signatures, which emerge as early
379 outcomes of metformin exposure.

380 ## 4. Discussion

381 Metformin is widely regarded as a promising compound with geroprotective potential (Barzilai et
382 al., 2016; Kulkarni et al., 2020) with a strong safety profile and therapeutic benefits beyond its
383 role as a first-line antidiabetic drug (Bu et al., 2022; Hua et al., 2023; Kasznicki et al., 2014;
384 Lashen, 2010; Rotermund et al., 2018). Yet, despite knowledge of individual metformin targets,
385 the pathways by which they converge to drive pro-longevity effects are not well understood.
386 Here, we provide a comprehensive genetic and cellular analysis of metformin-induced lifespan
387 extension in *S. cerevisiae*. Unexpectedly, we uncovered consistent gene–drug interactions
388 between metformin and chromatin-modifying factors, including several components of the
389 Set3C histone deacetylation complex. These results suggest that chromatin regulation is closely
390 associated with metformin's action on longevity. Notably, deletion of Set3C components
391 extended lifespan in untreated yeast cells but diminished the pro-longevity effect of metformin,
392 indicating convergence on shared pathways. To our knowledge, this is the first study linking
393 metformin's lifespan-extending effects to the Set3C histone deacetylation complex.

394 Aging is associated with heterochromatin loss and transcriptional activation of retrotransposable
395 elements, leading to increased expression and mobility in multiple organisms, including humans
396 (De Cecco et al., 2013; Hu et al., 2014; Li et al., 2013; Maxwell et al., 2011; Pal and Tyler, 2025;
397 Patterson et al., 2015; Wang et al., 2011). It has also been hypothesized that metformin could
398 act as a beneficial modulator of retrotransposon activity during embryological development
399 (Finley, 2018). Our transcriptomic data showed elevated retrotransposon RNA levels in
400 stationary-phase yeast cells; metformin further amplified this response, driving even higher
401 transcription of Ty1 elements. Nevertheless, their retromobility was moderately reduced,
402 suggesting a possible uncoupling of retrotransposon expression from their genome insertion.
403 This mirrors observations in Set3C gene-deletion mutants, which also exhibit increased Ty1

404 RNA but reduced integration events (Mou et al., 2006), pointing to retrotransposon regulation
405 as a shared outcome of Set3C impairment and metformin treatment.

406 The extent to which altered retrotransposon dynamics contribute causally to metformin-induced
407 longevity remains unclear. Nonetheless, Ty1 retrotransposition has been previously associated
408 with genome instability during chronological aging in yeasts (Maxwell et al., 2011). Further
409 supporting a potential causal role, ectopic expression of Ty1 extends CLS in a wild *S. paradoxus*
410 strain that naturally lacks retrotransposons, suggesting that retrotransposition can actively and
411 directly promote longevity (VanHoute and Maxwell, 2014). Our finding that metformin increases
412 Ty1 expression with minor effects in retromobility is consistent with recent studies in *Drosophila*
413 showing that changes in retrotransposon expression can affect aging independently of genomic
414 integration (Schneider et al., 2023). It also remains to be determined how metformin leads to
415 increased Ty1 expression. Notably, metformin increased the abundance of proteins involved in
416 mitochondrial function and in responses to ROS, both of which are known to modulate Ty1
417 dynamics in yeast (Stoycheva et al., 2007; VanHoute and Maxwell, 2014). Moreover, the Ty1-
418 transcriptional activator Tec1 and mitochondrial function compensate for each other's loss in
419 determining chronological aging (Cruz-Bonilla et al., 2025), further supporting a link between
420 metformin, stress responses, Ty1 regulation, and longevity in yeast.

421 By integrating large-scale genetic screening with proteomic and transcriptomic profiling, we
422 uncovered both canonical responses to metformin and an unexpected link between lifespan
423 extension, chromatin dynamics, and retrotransposon regulation. These findings expand the view
424 of metformin's cellular impact and its pro-longevity effects beyond metabolism and signaling
425 pathways. As retrotransposons are increasingly recognized for their roles in genome regulation
426 and stress adaptation, our study opens new avenues for exploring how metformin influences
427 these elements and how such regulation contributes to aging and longevity across species.

5. Authorship contribution statement

J.M-P. and A.D. conceptualized and designed the study. J.M-P, E.M-M., C.P-A. and M.M-F. performed experiments. J.M-P, D.A. and A.D. performed data analysis. S.F. and A.D. oversaw experiments. C.A-G. and A.D. oversaw data analysis. S.F. and A.D. acquired funding. J.M-P. and A.D. wrote the original draft. All authors read and critically revised the manuscript.

6. Funding

This work was funded by the Secretaría de Ciencia, Humanidades, Tecnología e Innovación de México (Secihti), Grants PN2016/ 2370 and CF-2023-I-1545. J.M-P. was funded by doctoral fellowship from Secihti (788970). E.M-M. was funded by a postdoctoral fellowship from Secihti (383325). A.D. was funded by a sabbatical fellowship from Secihti (26244).

7. Competing interest

The authors declare that they have no conflicts of interest with the contents of this article.

8. Acknowledgements

We thank J. A. Avelar-Rivas, S. E. Campos, and E. Mancera for critical reading of the manuscript and Y. Macotela and A. Moreno-Estrada for helpful discussions. The yeast Ty1-retromobility reporter was kindly shared by C. R. Landry's lab.

9. Data availability

All processed data are provided in the Supplementary Material accompanying this article. Raw RNAseq and flow cytometry data will be made available on NCBI GEO upon publication. The scripts used for data processing and analysis will be made available upon publication at https://github.com/.

449 ## Abbreviations

450 **C.F.U.:** Colony-forming units

451 **CFP:** Cerulean fluorescent protein

452 **CLS:** Chronological lifespan

453 **EDTA:** Ethylenediaminetetraacetic acid

454 **FDR:** False Discovery Rate

455 **GFP:** Green fluorescent protein

456 **GO:** Gene ontology

457 ***LE*:** Lifespan extension coefficient

458 **LTR:** Long Terminal Repeat

459 **MTF:** Metformin

460 **OD:** Optical density

461 **RFP:** Red fluorescent protein (mCherry)

462 ***S*:** Relative survival coefficient

463 **S.E.M.:** Standard error of the mean

464 **SC:** Synthetic complete

465 **Set3C:** Set3 complex

466 **SSC:** Side scatter

467 **WT:** Wild type

468 **YNB:** Yeast nitrogen base

469 **YPD:** Yeast-Extract Peptone Dextrose

470 ## References

471 Anisimov, V.N., Berstein, L.M., Egormin, P.A., Piskunova, T.S., Popovich, I.G., Zabezhinski, M.A.,
472 Tyndyk, M.L., Yurova, M. V., Kovalenko, I.G., Poroshina, T.E., Semenchenko, A. V., 2008.
473 Metformin slows down aging and extends life span of female SHR mice. Cell Cycle 7, 2769–
474 2773. https://doi.org/10.4161/cc.7.17.6625

475 Avelar-Rivas, J.A., Munguía-Figueroa, M., Juárez-Reyes, A., Garay, E., Campos, S.E., Shoresh,
476 N., DeLuna, A., 2020. An Optimized Competitive-Aging Method Reveals Gene-Drug
477 Interactions Underlying the Chronological Lifespan of Saccharomyces cerevisiae. Front Genet
478 11, 468. https://doi.org/10.3389/FGENE.2020.00468

479 Bannister, C.A., Holden, S.E., Jenkins-Jones, S., Morgan, C.Ll., Halcox, J.P., Schernthaner, G.,
480 Mukherjee, J., Currie, C.J., 2014. Can people with type 2 diabetes live longer than those
481 without? A comparison of mortality in people initiated with metformin or sulphonylurea
482 monotherapy and matched, non-diabetic controls. Diabetes Obes Metab 16, 1165–1173.
483 https://doi.org/https://doi.org/10.1111/dom.12354

484 Barzilai, N., Crandall, J.P., Kritchevsky, S.B., Espeland, M.A., 2016. Metformin as a Tool to Target
485 Aging. Cell Metab 23, 1060–1065. https://doi.org/10.1016/j.cmet.2016.05.011

486 Börklü, E., 2023. Insights from yeast: Transcriptional reprogramming following metformin treatment
487 is similar to that of deferiprone in a yeast Friedreich's ataxia model. Yeast 40, 143–151.
488 https://doi.org/10.1002/yea.3845

489 Borklu-Yucel, E., Eraslan, S., Ulgen, K.O., 2015. Transcriptional remodeling in response to transfer
490 upon carbon-limited or metformin-supplemented media in S. cerevisiae and its effect on
491 chronological life span. Appl Microbiol Biotechnol 99, 6775–6789.
492 https://doi.org/10.1007/s00253-015-6728-5

493 Brookman, J.L., Stott, A.J., Cheeseman, P.J., Adamson, C.S., Holmes, D., Cole, J., Burns, N.R.,
494 1995. Analysis of TYA Protein Regions Necessary for Formation of the Ty1 Virus-like Particle
495 Structure. Virology 212, 69–76. https://doi.org/https://doi.org/10.1006/viro.1995.1454

496 Bu, Y., Peng, M., Tang, X., Xu, X., Wu, Y., Chen, A.F., Yang, X., 2022. Protective effects of
497 metformin in various cardiovascular diseases: Clinical evidence and AMPK-dependent
498 mechanisms. J Cell Mol Med 26, 4886–4903.
499 https://doi.org/https://doi.org/10.1111/jcmm.17519

500 Burtner, C.R., Murakami, C.J., Kennedy, B.K., Kaeberlein, M., 2009. A molecular mechanism of
501 chronological aging in yeast. Cell Cycle 8, 1256–1270.
502 https://doi.org/https://doi.org/10.4161/cc.8.8.8287

503 Campbell, J.M., Bellman, S.M., Stephenson, M.D., Lisy., K., 2017. Metformin reduces all-cause
504 mortality and diseases of ageing independent of its effect on diabetes control: A systematic
505 review and meta-analysis. Ageing Res Rev 40, 31–44.
506 https://doi.org/https://doi.org/10.1016/j.arr.2017.08.003

507 Campos, S.E., Avelar-Rivas, J.A., Garay, E., Juárez-Reyes, A., DeLuna, A., 2018. Genomewide
508 mechanisms of chronological longevity by dietary restriction in budding yeast. Aging Cell 17,
509 e12749. https://doi.org/10.1111/acel.12749

510 Cruz-Bonilla, E., Campos, S.E., Funes, S., Abreu-Goodger, C., DeLuna, A., 2025. Exposing the
511 core genetic drivers of chronological aging in yeast cells. bioRxiv.
512 https://doi.org/https://doi.org/10.1101/2025.03.23.644847

513 De Cecco, M., Criscione, S.W., Peckham, E.J., Hillenmeyer, S., Hamm, E.A., Manivannan, J.,
514 Peterson, A.L., Kreiling, J.A., Neretti, N., Sedivy, J.M., 2013. Genomes of replicatively
515 senescent cells undergo global epigenetic changes leading to gene silencing and activation of
516 transposable elements. Aging Cell 12, 247–256.
517 https://doi.org/https://doi.org/10.1111/acel.12047

518 DeLuna, A., Springer, M., Kirschner, M.W., Kishony, R., 2010. Need-based up-regulation of protein
519 levels in response to deletion of their duplicate genes. PLoS Biol 8, e1000347.
520 https://doi.org/10.1371/journal.pbio.1000347

521 Fabrizio, P., Longo, V.D., 2003. The chronological life span of Saccharomyces cerevisiae. Aging
522 Cell 2, 73–81. https://doi.org/10.1046/J.1474-9728.2003.00033.X

523 Finley, J., 2018. Transposable elements, placental development, and oocyte activation: Cellular
524 stress and AMPK links jumping genes with the creation of human life. Med Hypotheses 118,
525 44–54. https://doi.org/https://doi.org/10.1016/j.mehy.2018.05.015

526 Foretz, M., Guigas, B., Viollet, B., 2023. Metformin: update on mechanisms of action and
527 repurposing potential. Nat Rev Endocrinol 19, 460–476. https://doi.org/10.1038/s41574-023-
528 00833-4

529 Garay, E., Campos, S.E., González de la Cruz, J., Gaspar, A.P., Jinich, A., DeLuna, A., 2014.
530 High-Resolution Profiling of Stationary-Phase Survival Reveals Yeast Longevity Factors and
531 Their Genetic Interactions. PLoS Genet 10, e1004168.
532 https://doi.org/10.1371/journal.pgen.1004168

533 Hénault, M., Marsit, S., Charron, G., Landry, C.R., 2020. The effect of hybridization on
534 transposable element accumulation in an undomesticated fungal species. Elife 9, e60474.
535 https://doi.org/10.7554/eLife.60474

536 Hu, Z., Chen, K., Xia, Z., Chavez, M., Pal, S., Seol, J.-H., Chen, C.-C., Li, W., Tyler, J.K., 2014.
537 Nucleosome loss leads to global transcriptional up-regulation and genomic instability during
538 yeast aging. Genes Dev 28, 396–408. https://doi.org/10.1101/gad.233221.113

539 Hua, Y., Zheng, Y., Yao, Y., Jia, R., Ge, S., Zhuang, A., 2023. Metformin and cancer hallmarks:
540 shedding new lights on therapeutic repurposing. J Transl Med 21, 403.
541 https://doi.org/10.1186/s12967-023-04263-8

542 Huh, W.-K., Falvo, J. V, Gerke, L.C., Carroll, A.S., Howson, R.W., Weissman, J.S., O'Shea, E.K.,
543 2003. Global analysis of protein localization in budding yeast. Nature 425, 686–691.
544 https://doi.org/10.1038/nature02026

545 Janssens, G.E., Veenhoff, L.M., 2016. Evidence for the hallmarks of human aging in replicatively
546 aging yeast. Microbial Cell. https://doi.org/10.15698/mic2016.07.510

547 Kaeberlein, M., 2010. Lessons on longevity from budding yeast. Nature 464, 513–519.
548 https://doi.org/10.1038/nature08981

549 Kasznicki, J., Sliwinska, A., Drzewoski, J., 2014. Metformin in cancer prevention and therapy. Ann
550 Transl Med. https://doi.org/10.3978/j.issn.2305-5839.2014.06.01

551 Kazi, R.S., Banarjee, R.M., Deshmukh, A.B., Patil, G. V, Jagadeeshaprasad, M.G., Kulkarni, M.J.,
552 2017. Glycation inhibitors extend yeast chronological lifespan by reducing advanced glycation
553 end products and by back regulation of proteins involved in mitochondrial respiration. J
554 Proteomics 156, 104–112. https://doi.org/https://doi.org/10.1016/j.jprot.2017.01.015

555 Kinsella, R.J., Kähäri, A., Haider, S., Zamora, J., Proctor, G., Spudich, G., Almeida-King, J.,
556 Staines, D., Derwent, P., Kerhornou, A., Kersey, P., Flicek, P., 2011. Ensembl BioMarts: a
557 hub for data retrieval across taxonomic space. Database 2011, bar030.
558 https://doi.org/10.1093/database/bar030

559 Kulkarni, Ameya S., Gubbi, S., Barzilai, N., 2020. Benefits of Metformin in Attenuating the
560 Hallmarks of Aging. Cell Metab 32, 15–30. https://doi.org/10.1016/j.cmet.2020.04.001

561 Lashen, H., 2010. Role of metformin in the management of polycystic ovary syndrome. Ther Adv
562 Endocrinol Metab. https://doi.org/10.1177/2042018810380215

563 Li, W., Prazak, L., Chatterjee, N., Grüninger, S., Krug, L., Theodorou, D., Dubnau, J., 2013.
564 Activation of transposable elements during aging and neuronal decline in Drosophila. Nat
565 Neurosci 16, 529–531. https://doi.org/10.1038/nn.3368

566 Ludovico, P., Sousa, M.J., Silva, M.T., Leão, C., Côrte-Real, M., 2001. Saccharomyces cerevisiae
567 commits to a programmed cell death process in response to acetic acid. Microbiology (N Y)
568 147, 2409–2415. https://doi.org/10.1099/00221287-147-9-2409

569 Ma, T., Tian, X., Zhang, B., Li, M., Wang, Y., Yang, C., Wu, J., Wei, X., Qu, Q., Yu, Yaxin, Long,
570 S., Feng, J.W., Li, C., Zhang, C., Xie, C., Wu, Y., Xu, Z., Chen, J., Yu, Yong, Huang, X., He,
571 Y., Yao, L., Zhang, L., Zhu, M., Wang, W., Wang, Z.C., Zhang, M., Bao, Y., Jia, W., Lin, S.Y.,
572 Ye, Z., Piao, H.L., Deng, X., Zhang, C.S., Lin, S.C., 2022. Low-dose metformin targets the
573 lysosomal AMPK pathway through PEN2. Nature 603, 159–165.
574 https://doi.org/10.1038/s41586-022-04431-8

575 Matecic, M., Smith, D.L., Pan, X., Maqani, N., Bekiranov, S., Boeke, J.D., Smith, J.S., 2010. A
576 microarray-based genetic screen for yeast chronological aging factors. PLoS Genet 6.
577 https://doi.org/10.1371/journal.pgen.1000921

578 Maxwell, P.H., Burhans, W.C., Curcio, M.J., 2011. Retrotransposition is associated with genome
579 instability during chronological aging. Proceedings of the National Academy of Sciences 108,
580 20376–20381. https://doi.org/10.1073/pnas.1100271108

581 Mou, Z., Kenny, A.E., Curcio, M.J., 2006. Hos2 and Set3 promote integration of Ty1
582 retrotransposons at tRNA genes in Saccharomyces cerevisiae. Genetics 172, 2157–2167.
583 https://doi.org/10.1534/genetics.105.054072

584 Newman, J.R.S., Ghaemmaghami, S., Ihmels, J., Breslow, D.K., Noble, M., DeRisi, J.L.,
585 Weissman, J.S., 2006. Single-cell proteomic analysis of S. cerevisiae reveals the architecture
586 of biological noise. Nature 441, 840–846. https://doi.org/10.1038/nature04785

587 Nyswaner, K.M., Checkley, M.A., Yi, M., Stephens, R.M., Garfinkel, D.J., 2008. Chromatin-
588 Associated Genes Protect the Yeast Genome From Ty1 Insertional Mutagenesis. Genetics
589 178, 197–214. https://doi.org/10.1534/genetics.107.082602

590 Onken, B., Driscoll, M., 2010. Metformin induces a dietary restriction-like state and the oxidative
591 stress response to extend C. elegans healthspan via AMPK, LKB1, and SKN-1. PLoS One 5.
592 https://doi.org/10.1371/journal.pone.0008758

593 Pal, S., Tyler, J.K., 2025. Epigenetics and aging. Sci Adv 2, e1600584.
594 https://doi.org/10.1126/sciadv.1600584

595 Patterson, M.N., Scannapieco, A.E., Au, P.H., Dorsey, S., Royer, C.A., Maxwell, P.H., 2015.
596 Preferential retrotransposition in aging yeast mother cells is correlated with increased genome
597 instability. DNA Repair (Amst) 34, 18–27.
598 https://doi.org/https://doi.org/10.1016/j.dnarep.2015.07.004

599 Pernicova, I., Korbonits, M., 2014. Metformin-Mode of action and clinical implications for diabetes
600 and cancer. Nat Rev Endocrinol. https://doi.org/10.1038/nrendo.2013.256

601 Pijnappel, W.W.M.P., Schaft, D., Roguev, A., Shevchenko, A., Tekotte, H., Wilm, M., Rigaut, G.,
602 Séraphin, B., Aasland, R., Stewart, A.F., 2001. The S. cerevisiae SET3 complex includes two
603 histone deacetylases, Hos2 and Hst1, and is a meiotic-specific repressor of the sporulation
604 gene program. Genes Dev 15, 2991–3004. https://doi.org/10.1101/gad.207401

605 Rena, G., Hardie, D.G., Pearson, E.R., 2017. The mechanisms of action of metformin.
606 Diabetologia. https://doi.org/10.1007/s00125-017-4342-z

607 Roberts, T.M., Rudolf, F., Meyer, A., Pellaux, R., Whitehead, E., Panke, S., Held, M., 2016.
608 Identification and Characterisation of a pH-stable GFP. Sci Rep 6.
609 https://doi.org/10.1038/srep28166

610 Rotermund, C., Machetanz, G., Fitzgerald, J.C., 2018. The therapeutic potential of metformin in
611 neurodegenerative diseases. Front Endocrinol (Lausanne).
612 https://doi.org/10.3389/fendo.2018.00400

613 Ryu, H.-Y., 2024. Histone Modification Pathways Suppressing Cryptic Transcription. Epigenomes
614 8. https://doi.org/10.3390/epigenomes8040042

615 Schneider, B.K., Sun, S., Lee, M., Li, W., Skvir, N., Neretti, N., Vijg, J., Secombe, J., 2023.
616 Expression of retrotransposons contributes to aging in Drosophila. Genetics 224, iyad073.
617 https://doi.org/10.1093/genetics/iyad073

618 Seylan, C., Tarhan, Ç., 2023. Metformin extends the chronological lifespan of fission yeast by
619 altering energy metabolism and stress resistance capacity. FEMS Yeast Res 23.
620 https://doi.org/10.1093/femsyr/foad018

621 Sheff, M.A., Thorn, K.S., 2004. Optimized cassettes for fluorescent protein tagging in
622 Saccharomyces cerevisiae. Yeast 21, 661–670. https://doi.org/10.1002/YEA.1130

623 Stancu, A.L., 2015. AMPK activation can delay aging. Discoveries 3, e53.
624 https://doi.org/10.15190/d.2015.45

625 Stevenson-Hoare, J., Leonenko, G., Escott-Price, V., 2023. Comparison of long-term effects of
626 metformin on longevity between people with type 2 diabetes and matched non-diabetic
627 controls. BMC Public Health 23, 804. https://doi.org/10.1186/s12889-023-15764-y

628 Stoycheva, T., Massardo, D.R., Pesheva, M., Venkov, P., Wolf, K., Del Giudice, L., Pontieri, P.,
629 2007. Ty1 transposition induced by carcinogens in Saccharomyces cerevisiae yeast depends
630 on mitochondrial function. Gene 389, 212–218.
631 https://doi.org/https://doi.org/10.1016/j.gene.2006.11.009

632 Stynen, B., Abd-Rabbo, D., Kowarzyk, J., Miller-Fleming, L., Aulakh, S.K., Garneau, P., Ralser, M.,
633 Michnick, S.W., 2018. Changes of Cell Biochemical States Are Revealed in Protein

634 Homomeric Complex Dynamics. Cell 175, 1418-1429.e9.
635 https://doi.org/10.1016/j.cell.2018.09.050

636 VanHoute, D., Maxwell, P.H., 2014. Extension of Saccharomyces paradoxus Chronological
637 Lifespan by Retrotransposons in Certain Media Conditions Is Associated with Changes in
638 Reactive Oxygen Species. Genetics 198, 531–545.
639 https://doi.org/10.1534/genetics.114.168799

640 Wang, J., Geesman, G.J., Hostikka, S.L., Atallah, M., Blackwell, B., Lee, E., Cook, P.J., Pasaniuc,
641 B., Shariat, G., Halperin, E., Dobke, M., Rosenfeld, M.G., Jordan, I.K., Lunyak, V. V, 2011.
642 Inhibition of activated pericentromeric SINE/Alu repeat transcription in senescent human adult
643 stem cells reinstates self-renewal. Cell Cycle 10, 3016–3030.
644 https://doi.org/10.4161/cc.10.17.17543

645 Yang, Y., Lu, X., Liu, N., Ma, S., Zhang, H., Zhang, Z., Yang, K., Jiang, M., Zheng, Z., Qiao, Y., Hu,
646 Q., Huang, Y., Zhang, Y., Xiong, M., Liu, L., Jiang, X., Reddy, P., Dong, X., Xu, F., Wang, Q.,
647 Zhao, Q., Lei, J., Sun, S., Jing, Ying, Li, J., Cai, Y., Fan, Y., Yan, K., Jing, Yaobin, Haghani,
648 A., Xing, M., Zhang, X., Zhu, G., Song, W., Horvath, S., Rodriguez Esteban, C., Song, M.,
649 Wang, S., Zhao, G., Li, W., Izpisua Belmonte, J.C., Qu, J., Zhang, W., Liu, G.-H., 2024.
650 Metformin decelerates aging clock in male monkeys. Cell 187, 6358-6378.e29.
651 https://doi.org/10.1016/j.cell.2024.08.021

652 Zhang, H., Chen, J., Ou, Y., Li, Y., Hu, S., Shao, L.-W., Liu, Y., 2017. Metformin extends C.
653 elegans lifespan through lysosomal pathway. Elife.
654 https://doi.org/https://doi.org/10.7554/eLife.31268

655 Zhou, G., Myers, R., Li, Y., Chen, Y., Shen, X., Fenyk-Melody, J., Wu, M., Ventre, J., Doebber, T.,
656 Fujii, N., Musi, N., Hirshman, M.F., Goodyear, L.J., Moller, D.E., 2001. Role of AMP-activated
657 protein kinase in mechanism of metformin action. Journal of Clinical Investigation 108, 1167–
658 1174. https://doi.org/10.1172/jci200113505

659 Zimmermann, A., Hofer, S., Pendl, T., Kainz, K., Madeo, F., Carmona-Gutierrez, D., 2018. Yeast
660 as a tool to identify anti-aging compounds. FEMS Yeast Res.
661 https://doi.org/10.1093/femsyr/foy020

662

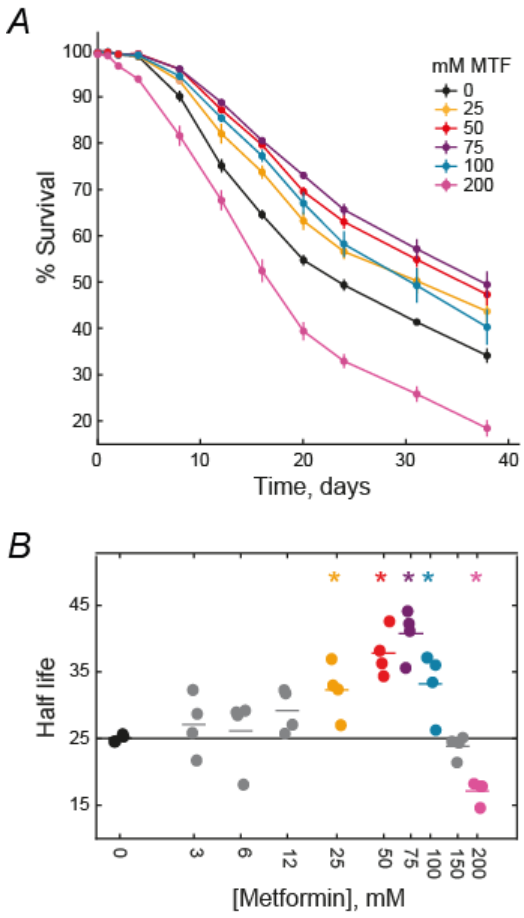

Figure 1. Metformin extends CLS in a dose-dependent manner. *A*) The WT strain was aged with increasing metformin concentrations in SC medium buffered at pH 4 and survival was tracked by live and death staining coupled with flow cytometry. The plot shows only those treatments that resulted in increased or decreased CLS. Error bars are the S.E.M. (n=4). ***B*)** Survival half-lives were estimated by fitting the survival data to an exponential decay model; asterisks indicate treatments that were statistically different to the control without metfrormin (p<0.05, unpaired two-tailed t-test).

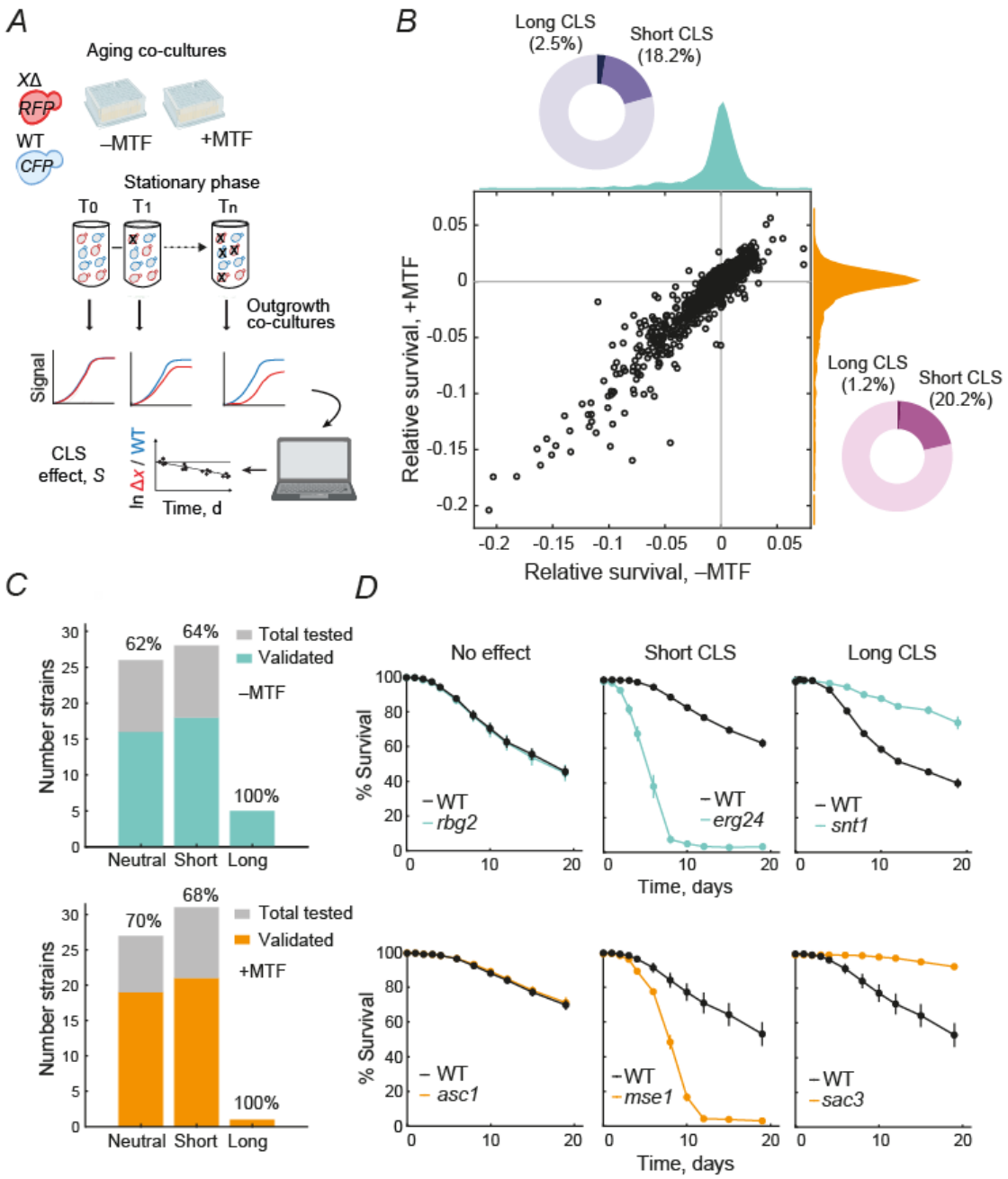

Figure 2. **High-resolution genetic screening of lifespan extension by metformin.** ***A)*** Schematic representation of the competitive method used to test the effect of metformin on *CLS*. Saturated cultures of *RFP*-labeled deletion strains and *CFP*-labeled *WT* strain are mixed and inoculated into SC medium without metformin (–MTF) or 50 mM metformin (+MTF). Samples of the aging co-cultures are taken over the days and inoculated in a fresh medium. The outgrowth kinetics are monitored by recording the optical density and tracking the fluorescence signals. The collected data is fitted to a multiple linear regression model to estimate the relative survival coefficient (CLS effect, *S*) for each mutant tested. ***B)*** The scatter plot displays the relative survival coefficients of 1438 knockout strains of human ortholog

genes aged in a medium without metformin (–MTF, horizontal axis) and supplemented with 50 mM MTF (+MTF, vertical axis). The orange and cyan histograms correspond to the distribution of the survival coefficients in –MTF and +MTF, respectively. Pie charts display the percentage of long and short CLS strains detected in each treatment. CLS phenotypes were identified through *Z*-score estimation, by comparing the mutant´s survival coefficient to the survival distribution of 227 wild-type reference strains. A multiple-testing correction was then applied to define hits at a 5% FDR (Benjamini–Hochberg). ***C*)** Percentage of validated strains by live and death assay shown by CLS phenotype in –MTF (cyan) and +MTF (orange). ***D*)** Representative survival curves obtained by live and dead assays of short, long and neutral strains compared to a wild-type strain (black line) aged in –MTF (cyan lines) or +MTF (orange lines). Error bars are the S.E.M. (*n*=5).

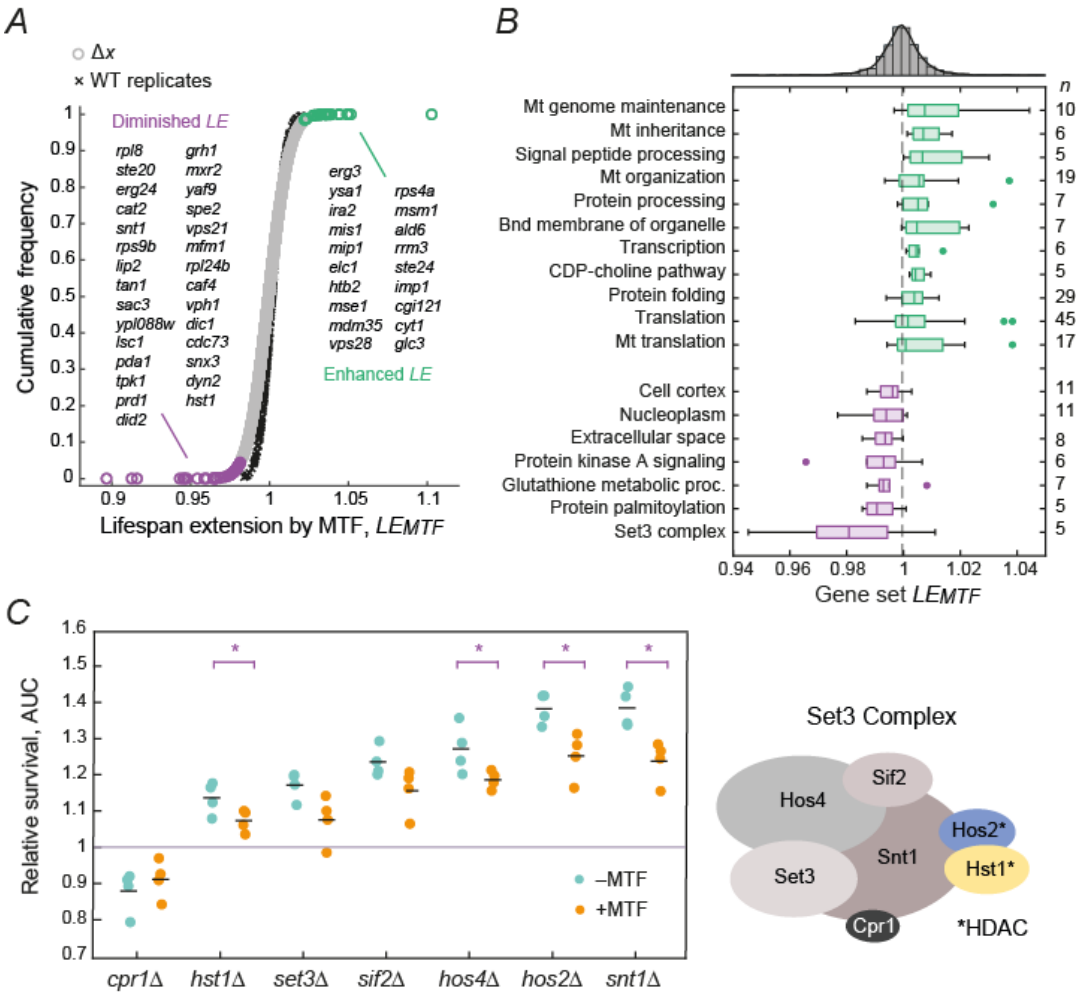

Figure 3. Genetic interactions underlying metformin-induced longevity. *A*) Lifespan extension by metformin, LE_{MTF}, was calculated for each mutant (grey circles) and compared to the LE_{MTF} distribution of WT strains (black crosses) to score statistical significance at 5% FDR (highlighted in purple and green for diminished and enhanced CLS extension, respectively). Top hits (1% FDR) are displayed in the plot. ***B*)** The boxplots show the LE_{MTF} (horizontal axis) of genes annotated within the same GO term (vertical axis); *Mt* indicates mitochondrial-related categories. CLS specific gene groups exhibiting an increase in median lifespan are plotted in green, while gene groups with a reduced median LE_{MTF} are shown in purple (Wilcoxon rank sum test). The dashed gray line is the median LE_{MTF} of all strains tested (n = 1438), while the histogram on the top shows the data distribution of the entire dataset. ***C*)** Validation of hits for genes encoding subunits of Set3C. Replicates of single and double mutants were aged in individual cultures, and survival curves were obtained using live/dead staining of stationary-phase cultures at different days. The plot shows the area under the curve (AUC) for the mutants, expressed relative to the average AUC of the WT aged in –MTF (cyan) or +MTF treatment (orange). Statistical differences between each treatment pair

were assessed by unpaired two-tailed *t*-test (*$p<0.05$). Set3C schematic adapted from (Ryu, 2024); asterisks indicate protein subunits with annotated histone deacetylase activity.

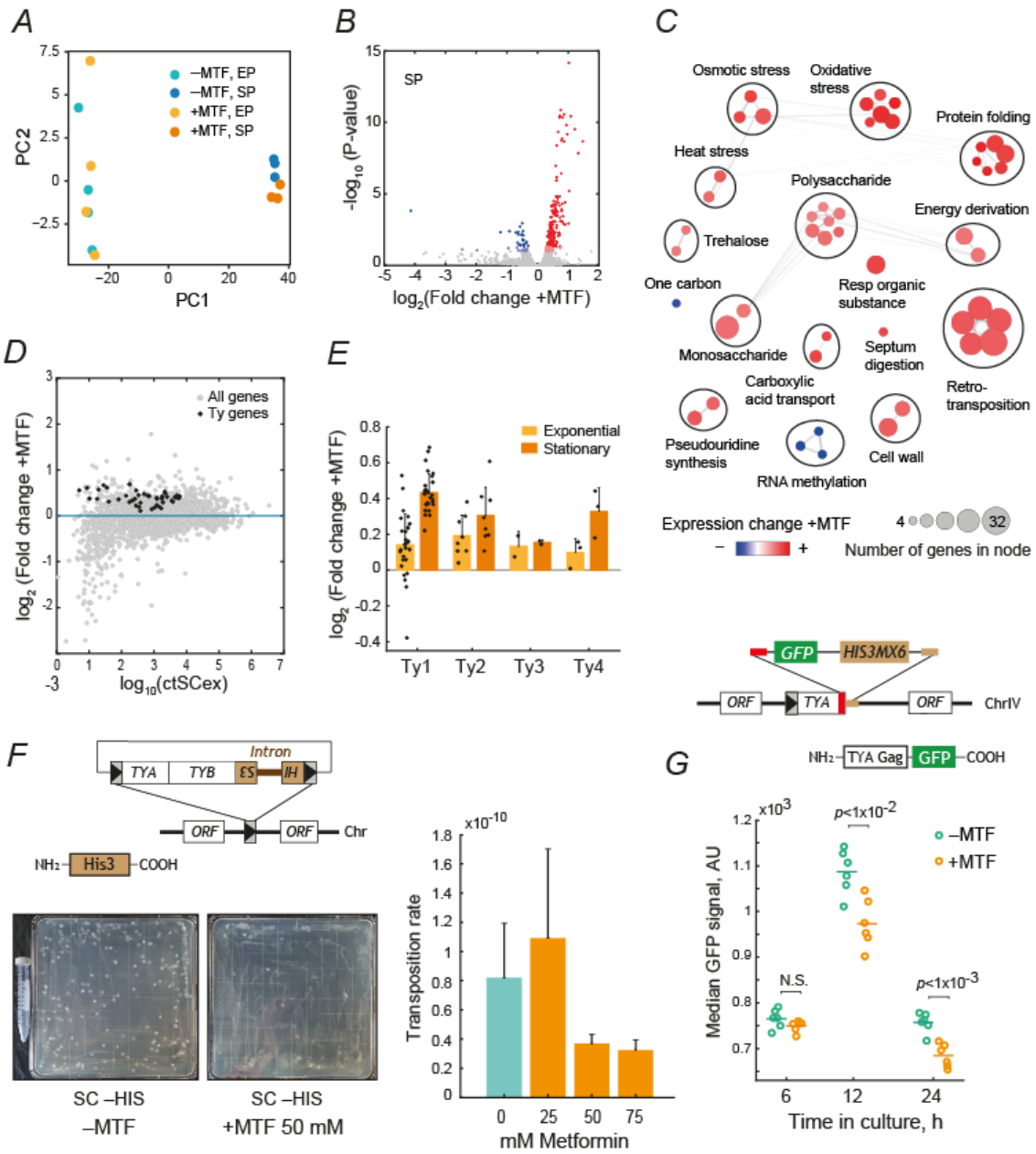

Figure 4. Changes in retrotransposon dynamics in response to metformin. ***A)*** Principal component analysis (PCA) of gene expression data of exponential (EP, *n*=3) and stationary phase groups (SP, *n*=4) without metformin (–MTF) and treated with 50 mM metformin (+MTF). ***B)*** Volcano plot showing the differential expresses genes in response to 50 mM of metformin treatment (+MTF) in late stationary phase cells. Colored circles correspond to upregulated (red), or downregulated (blue) genes detected by DESeq2 analysis using a strict ($p<0.05$, dark dots) or lenient cutoff ($p<0.1$, light dots) after FDR correction. ***C)*** Functional clustering of upregulated (red) and downregulated (blue) genes group by mega-clusters. An enrichment analysis was conducted with differentially expressed genes. The network results from the functional clustering of biological processes found by similarity between groups. Each cluster

is delimited by a circle and contains related gene groups. Node size represents the number of genes in the group. The width edge is constructed with the similarity Jaccard index estimated between groups. ***D)*** The scatter plot compares the expression of genes (gray) in response to metformin with its basal expression (expression in –MTF medium on exponential phase). Black points correspond to the Ty1 retrotransposon genes detected. ***E)*** Fold change of Ty retrotransposon families in exponential and stationary phase. ***F)*** Ty1 retromobility was measured employing a Ty1*his-AI* reporter strain treated with 0, 25, and 50 mM of metformin (n=14 for 0 and 50 mM and n=7 for 25 mM; t-test). **G)** The median intensity fluorescence of a Gag-GFP fusion was tracked at different time points (6, 12, and 24 h) in response to 0 or 50 mM of metformin (n= 6; t-test).

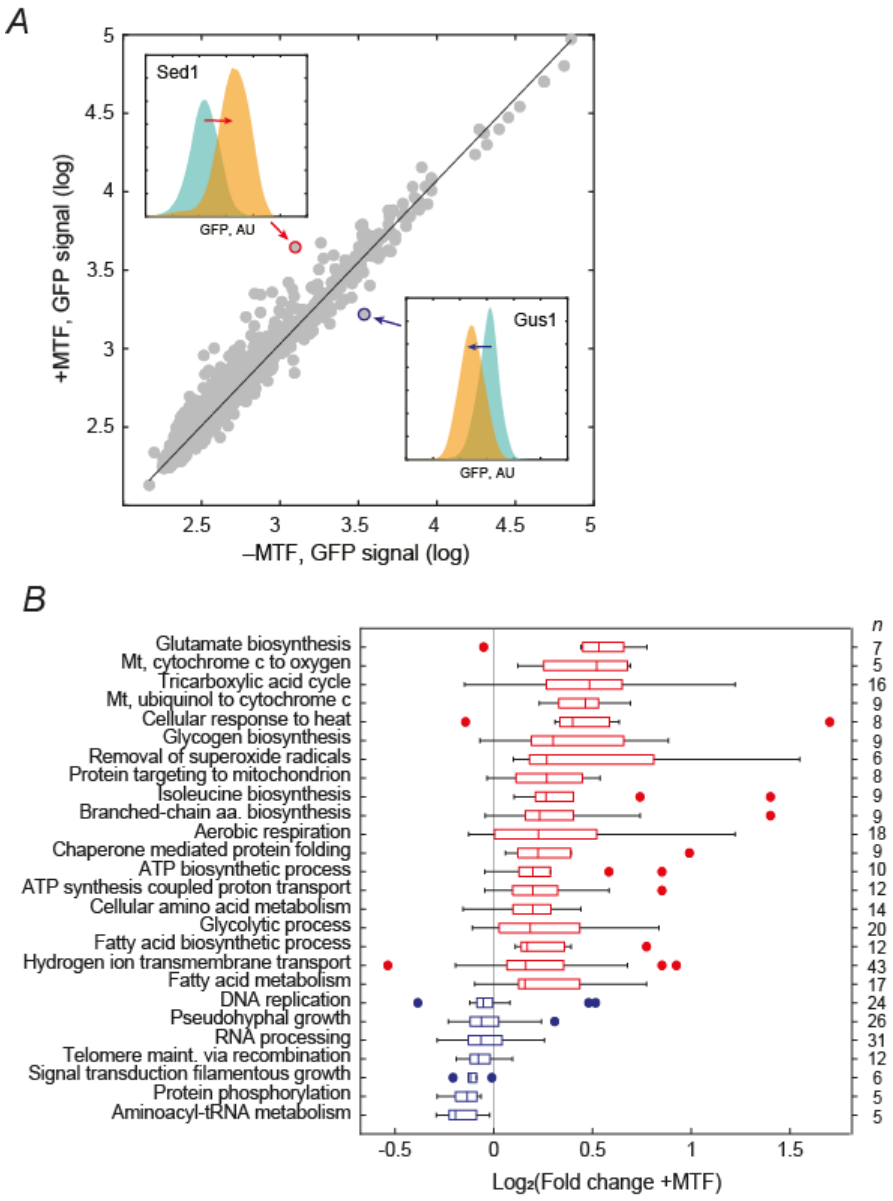

Figure 5. Proteomic response to metformin. ***A)*** Scatter plot of the GFP signal of 2616 fusion strains under no metformin (–MTF, horizontal axis) and 50 mM metformin (+MTF, vertical axis), measured by flow cytometry. Insets show the GFP signal distribution of Sed1 and Gus1 in a media supplemented without metformin (cyan) and with 50 mM metformin (orange). ***B)*** Box plots show the fold-change distribution of the functional groups that change their abundance in response to metformin treatment (p<0.05, Wilcoxon rank sum test).

Apendix A. Supplementary Material

Metformin-induced longevity is associated with retrotransposon dynamics in yest chronological aging.

Supplementary Tables

Table S1. Competitive aging output data and statistics (XLSX FILE)

Table S2. CLS-specific gene groups associated with metformin-induced longevity (XLSX FILE)

Table S3. RNASeq transcriptomic output data and statistics (XLSX FILE)

Table S4. GO enrichment analysis, RNAseq transcriptomics (XLSX FILE)

Table S5. GFP-fusions proteomic output data (XLSX FILE)

Supplementary Figures

Figures S1–S5

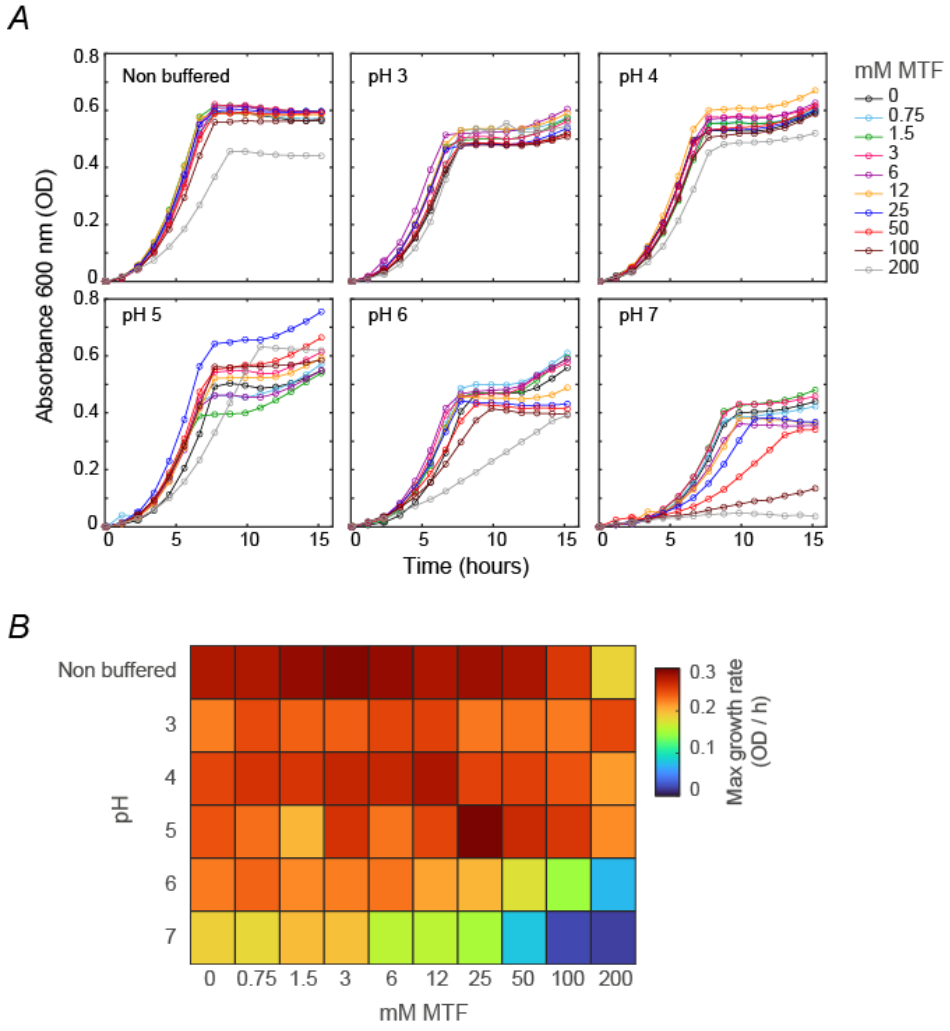

Supplementary Figure S1. ***A*)** Plots show growth kinetics of the WT strain at increasing concentrations of metformin, assayed from culture growth in non-buffered and buffered media adjusted at different pHs. ***B*)** Heatmap shows the maximum growth rates observed at increasing concentrations of metformin (horizontal axis) under different pH conditions (vertical axis).

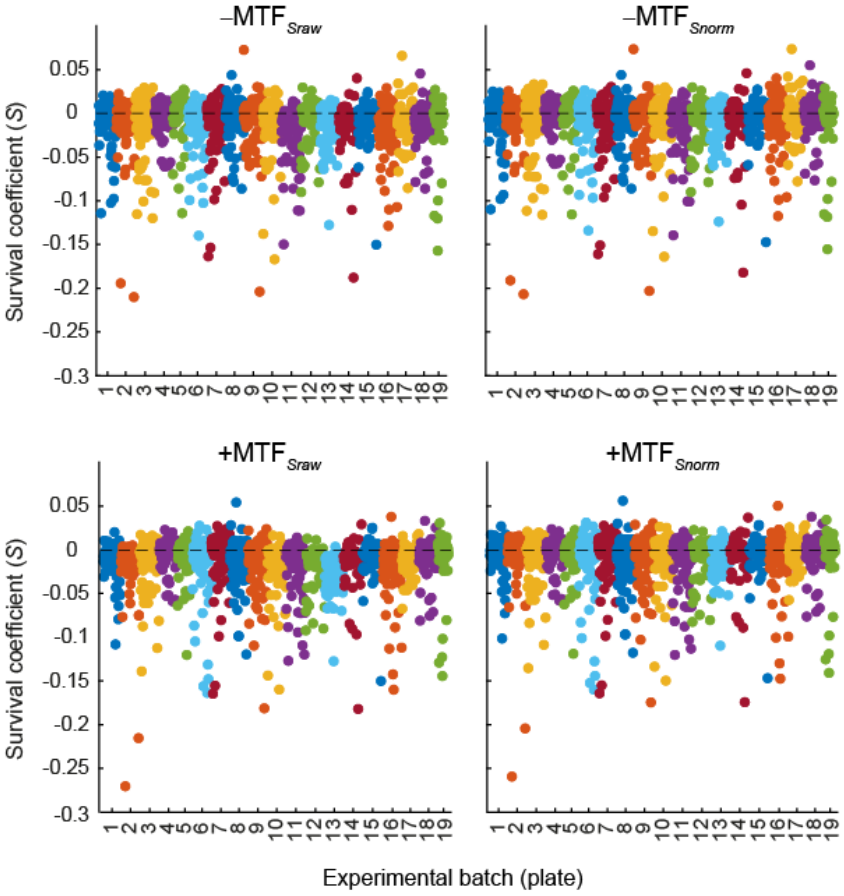

Supplementary Figure S2. Raw (left panels) and normalized (right panels) survival coefficients (*S*) are plotted per plate for 0 mM (–MTF) and 50 mM MTF (+MTF). To correct batch effects, data was normalized by subtracting the median *S* of each plate from the *S* of the mutants of the same plate, including WT reference replicates.

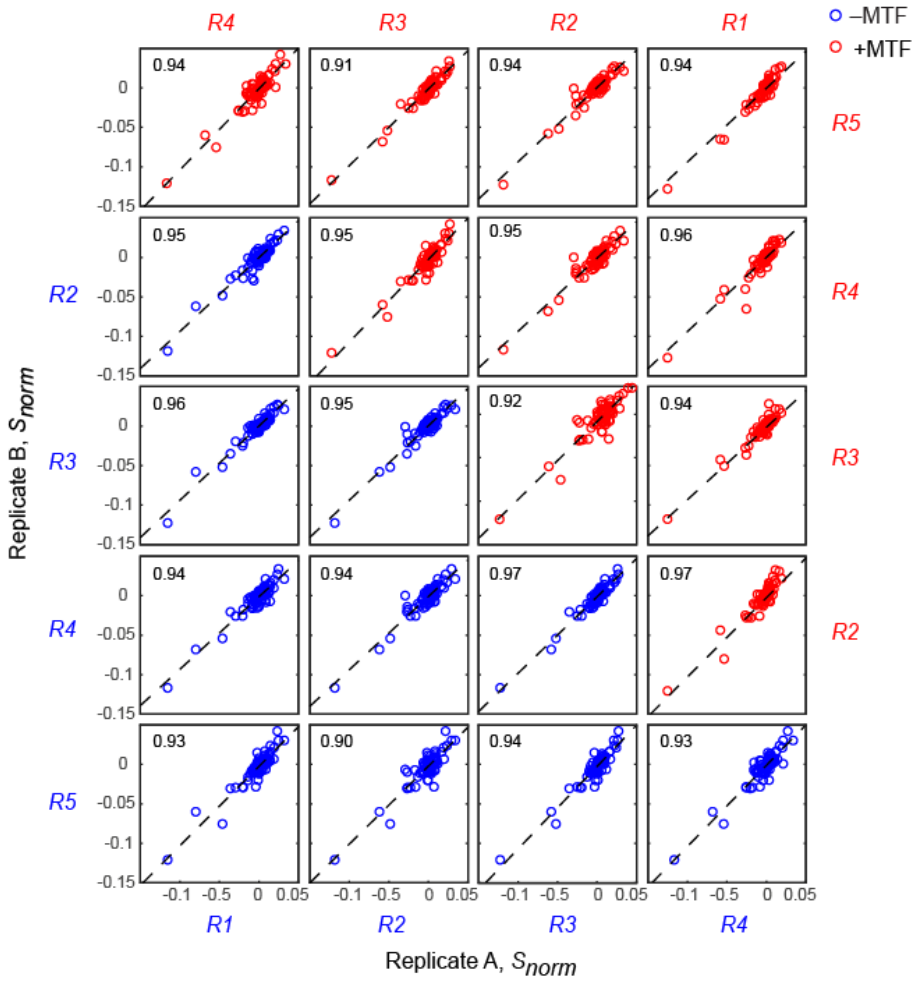

Supplementary Figure S3. Scatterplot matrices of the survival coefficients of 84 mutants replicated in different batches to assess the replicability of our phenotyping approach. Each scatter plot also shows the correlation coefficient estimated for every replicate comparison (Pearson). Blue dots correspond to the 0 mM treatment (–MTF) and red dots to 50 mM MTF (+MTF).

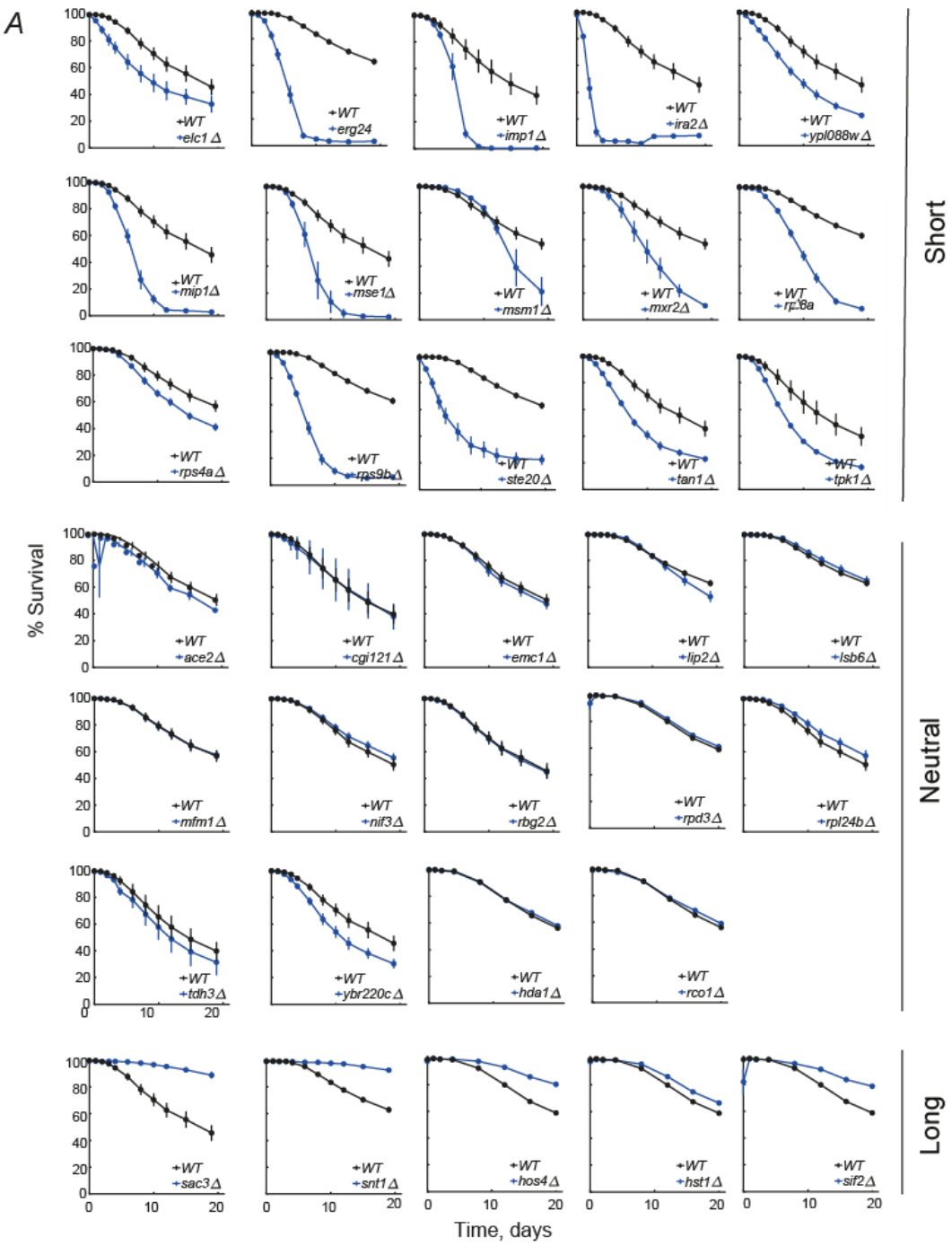

Supplementary Figure S4. ***A)*** Validation of CLS phenotypes in –MTF. Survival curves of selected mutant strains (blue lines, *n* = 5) were compared to WT (black lines) by live and death assay coupled to analytical cytometry. Error bars indicate the S.E.M. Upper and lower panels show short- and long-lived hits from the genetic screening, while middle panels show non-significant (neutral) phenotypes.

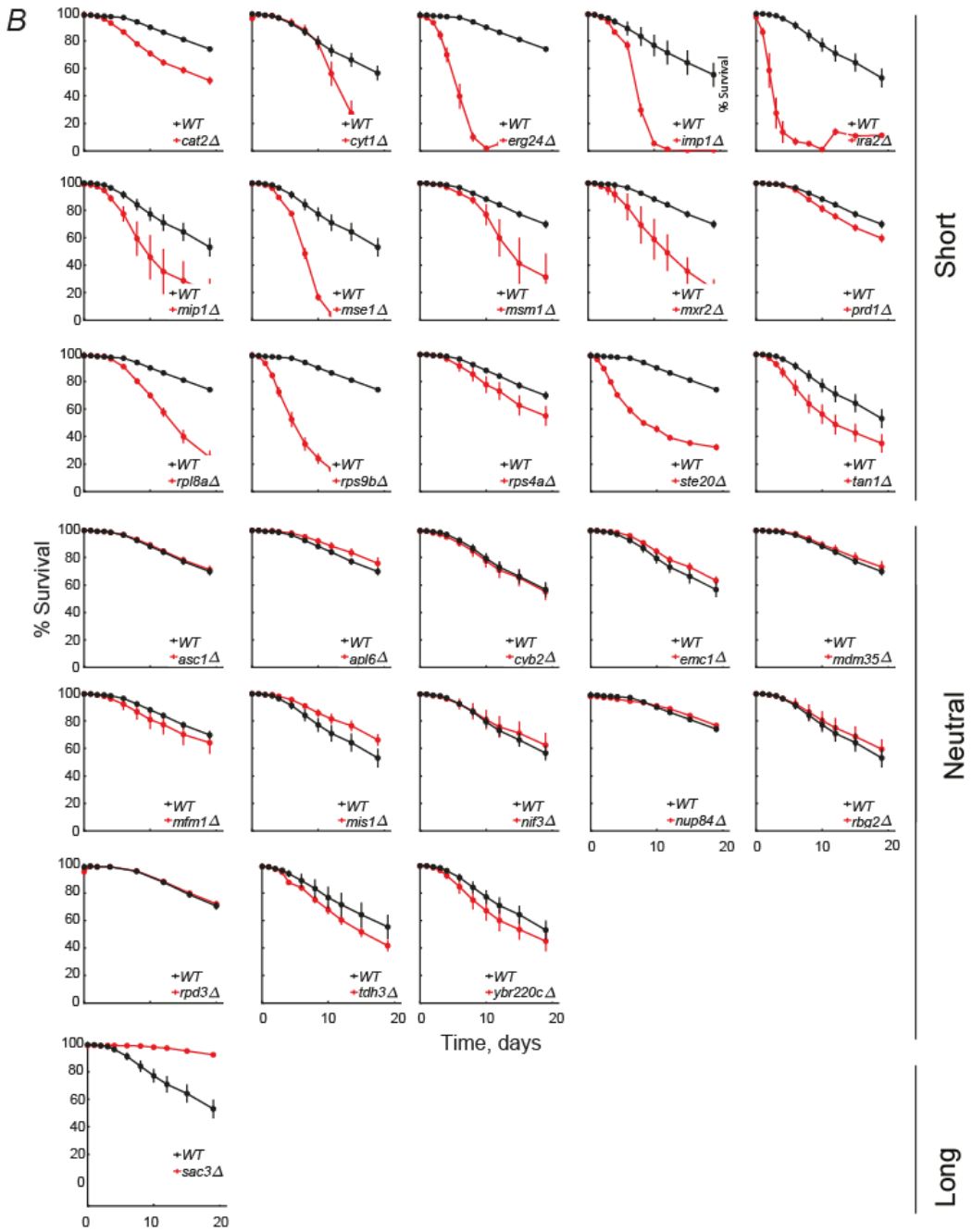

Supplementary Figure S4. ***B)*** Validation of CLS phenotypes in +MTF. Survival curves of selected mutant strains (red lines, *n* = 5) were compared to WT (black lines) by live and death assay coupled to analytical cytometry. Error bars indicate the S.E.M. Upper and lower panels show short- and long-lived hits from the genetic screening, while middle panels show non-significant (neutral) phenotypes.

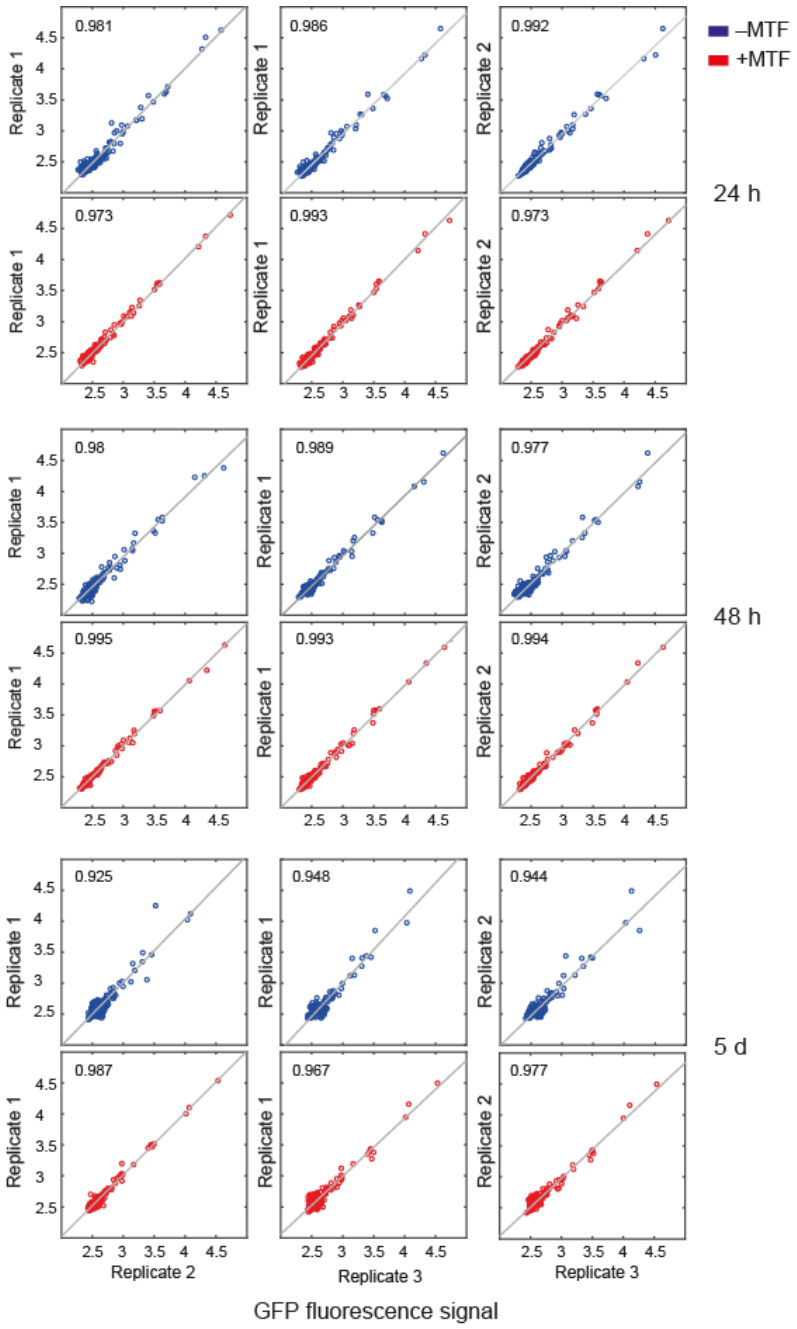

Supplementary Figure S5. Scatterplot matrices of the median intensity fluorescence of 2616 GFP fusion strains replicated in different batches to assess the replicability of our method through time (24h, 48h and 5 days). Each scatter plot also shows the correlation coefficient estimated for every replicate comparison (Pearson). Expression levels in the no metformin (–MTF) and 50 mM metformin (+MTF) treatments are shown in blue and red circles, respectively.